APPLIED ORGANOMETALLIC CHEMISTRY
Appl. Organometal. Chem. 2001; **15**: 113–120

Recent developments in electrochemical and photoelectrochemical CO_2 reduction: involvement of the $(CO_2)_2^{\bullet-}$ dimer radical anion†

Donald A. Tryk,[1] Toshio Yamamoto,[1] Masahide Kokubun,[1] Kouske Hirota,[1] Kazuhito Hashimoto,[2] Masafumi Okawa[3] and Akira Fujishima[1]*
[1]Department of Applied Chemistry, School of Engineering, The University of Tokyo, 7-3-1 Hongo, Bunkyo-ku, Tokyo 113-8656, Japan
[2]Research Center for Advanced Science and Technology, The University of Tokyo, 4-6-1 Komaba, Meguro-ku, Tokyo 153-8904, Japan
[3]Electric Power Development Company, Limited, 6-15-1, Ginza, Chuo-ku, Tokyo 104-8165, Japan

Electrochemical CO_2 reduction was examined on high-area transition metal catalysts supported on nanoporous activated carbon fiber (ACF) supports, in the form of gas diffusion electrodes, in aqueous $KHCO_3$ solution. The most active catalyst was ACF/Ni, on which up to *ca* 65 mA cm^{-2} current density for CO production was observed, with simultaneous production of hydrogen of *ca* 15 mA cm^{-2} at −1.6 V vs SCE. At more negative potentials, higher H_2/CO ratios can be obtained. The reaction mechanism for CO production probably involves a chemical reaction between CO_2 and the radical anion $CO_2^{\bullet-}$ to produce the CO_2 dimer radical anion $(CO_2)_2^{\bullet-}$. The results are compared with those for photoelectrochemical CO_2 reduction on p-InP, on which the mechanism is thought to involve the one-electron reduction of two adsorbed CO_2 molecules to produce the CO_2 dimer radical anion. **Copyright © 2001 John Wiley & Sons, Ltd.**

Keywords: CO_2 reduction; radical ions; nanospace effect; nanoparticulate catalysts

INTRODUCTION

The electrochemical reduction of CO_2 to produce fuels or chemical feedstocks may be a useful approach towards the utilization of this ubiquitous carbon source, particularly if solar electrical power can be used. The electrochemical approach has the advantage that water can be used as the proton source.[1] Separate solar energy harvesting and CO_2 reductions systems can be used, e.g. a photovoltaic cell plus an electrochemical cell, or an integrated system can be used, i.e. a photoelectrochemical cell. However, in both cases it is important to achieve high current densities, low polarization, and high selectivity for CO_2 reduction compared with other possible reactions, such as hydrogen evolution.

In our laboratory, we have been examining both electrochemical and photoelectrochemical approaches. For the electrochemical approach, we have focused on gas diffusion electrodes (GDEs), specifically those employing metallic catalysts on nanoporous supports. We have found that the selectivity for CO_2 reduction vs hydrogen evolution is enhanced with these catalysts, presumably due to enhanced CO_2 adsorption in the nanopores. The effect is similar to that of high pressure. Of several metals examined, including iron, nickel, copper, and palladium, the highest performance was obtained for nickel, for which an unprecedented 65% current efficiency for CO production was obtained.

GDEs have been used extensively in order to achieve high current densities for CO_2 reduction, with partial current densities up to several hundreds of milliamps per square centimeter having been

* Correspondence to: Akira Fujishima, Department of Applied Chemistry, School of Engineering, The University of Tokyo, 7-3-1 Hongo, Bunkyo-ku, Tokyo 113-8656, Japan.
Contract/grant sponsor: Ministry of Education, Science, Sports and Culture of Japan.
Contract/grant sponsor: International Joint Research Program of New Energy.
Contract/grant sponsor: Industrial Technology Development Organization (NEDO).
† This paper is based on work presented at the Fifth International Conference on Carbon Dioxide Utilization (ICCDU V), held on 5–10 September 1999 at Karlsruhe, Germany.

Copyright © 2001 John Wiley & Sons, Ltd.

reached.[2–14] We have recently been pursuing the idea of using nanoporous catalyst supports, such as activated carbon fibers (ACFs), on which CO_2 is known to exhibit enhanced adsorption.[15,16] Within nanometer-scale pores, so-called nanospace effects, i.e. effective high-pressure reaction conditions (over 20 MPa), are known to exist.[17] In the present work, we combine the ideas of nanospace and GDEs in order to try to obtain the benefits of high-pressure conditions at ambient pressure for CO_2 reduction.[18] We have examined the electrochemical reduction of CO_2 with GDEs based upon nanoporous ACFs, with deposited metals, such as nickel, iron, palladium, and copper as electrocatalysts and have obtained evidence that indeed such high-pressure effects occur at ambient pressure in an electrochemical system.

We have also been interested in the use of semiconducting p-type diamond electrodes for CO_2 reduction, because hydrogen evolution is extremely inhibited on such surfaces.[19] Indeed, using methanol as the solvent with high-pressure CO_2, we found that essentially no hydrogen was produced; CO, methyl formate and hydrocarbons were the major products. This is quite unusual—in our previous work, we found that most metal electrodes produce substantial amounts of hydrogen, the main exception being silver.[20–23]

Regarding the photoelectrochemical approach, we have obtained high current densities for CO_2 to CO at relatively low overpotentials at p-InP photoelectrodes in methanol with high-pressure CO_2.[24,25] There is a shift in the positive direction of *ca* 0.6 V due to photoassisted charge separation, and there also appears to be a strong catalytic effect, which is responsible for an additional shift of *ca* 1.1 V. We propose that this effect is due to the stabilization of the $CO_2^{\cdot -}$ radical anion by formation of an adduct with neutral CO_2. This effect is dependent upon the high CO_2 pressure, which probably enhances the adsorption of CO_2 on the electrode surface. There are two additional benefits of high CO_2 pressure: first, the very low current efficiency for hydrogen evolution, and, second, the high resistance to photocorrosion.

METHODS

GDE measurements

High purity ACFs (type KF-1500; surface area, 1400 to 1500 $m^2\ g^{-1}$) were obtained from Toyobo Co., Ltd (Osaka, Japan). The detailed procedures for the preparation of ACF-supported metal catalysts are given in a separate publication.[26] Briefly, the fibers were placed in contact with aqueous solutions of the metal nitrates and were stirred at room temperature for *ca* 10 h. After washing with water and drying, the fibers were heated-treated under hydrogen at 350 °C. In one method (A) for making PTFE-bonded GDE active layers containing acetylene black as a matrixing agent, the ACF content was 3 mg cm^{-2}. A second method (B), was used to prepare more highly loaded electrodes (ACF, 14 mg cm^{-2}). A three-compartment cell was used for the electrochemical measurements. CO_2 was fed into the gas compartment; 0.5 M $KHCO_3$ aqueous solution was used as the electrolyte. Oxygen was removed before the electrolysis. A saturated calomel electrode (SCE) and a platinum wire were used as the reference electrode and counter electrode respectively. The electrode potential was corrected using an I–R compensator (Hokuto HI-203). The reduction products were analyzed by gas chromatography and high performance liquid chromatography.

Photoelectrochemical measurements

Detailed experimental procedures are given in a separate publication.[25] p-Type InP [(100), 2×10^{18} cm^{-3}], p-GaAs [(100), $(1–5) \times 10^{17}$ cm^{-3}], and p-Si [(100), 10–50 Ω] were used as electrodes. A silver wire quasi-reference electrode (Ag QRE, *ca* + 80 mV vs SCE and −310 mV vs Fc/Fc^+) was used. A platinum wire was used as the counter electrode. The p-InP and p-GaAs electrodes were etched by dipping in boiling aqua regia for *ca* 5 s before each experiment. The p-Si electrodes were treated first in a mixture of 5% HF, acetic acid and 10% nitric acid, and finally in 10% HF–ethanol solution, each for *ca* 30 s.

The equipment and the procedures used in the experiments with the CO_2–methanol medium have been described in previous papers.[20,22] The cell consisted of a stainless steel pressure vessel equipped with a 2 cm thick quartz window. The electrolyte solution [3 cm^3, 0.3 M tetrabutylammonium perchlorate (TBAP, reagent grade) in CH_3OH] was placed in a glass cell liner in the stainless steel vessel. CO_2 was introduced into the pressure vessel at the designated pressures (1 to 40 atm). In control experiments, 1 atm argon was used.

A 500 W xenon lamp was used to illuminate the semiconductor photocathode. After filtering wave-

Copyright © 2001 John Wiley & Sons, Ltd.

lengths shorter than 370 nm, the intensity of the lamp output was found to be 480 mW cm^{-2} at the electrode surface. Ohmic loss was measured, and corrections were performed mathematically on the current–potential curves.

During the photoelectrolyses, total amounts of charge from 1 to 10 C were passed galvanostatically at 1 to 100 mA cm^{-2} using a potentiostat–galvanostat. After the electrolysis, the gas- and liquid-phase products were analyzed using gas chromatography with either a flame ionization detector or a thermal conductivity detector.

In the case of the preliminary electrochemical measurements with diamond film electrodes, similar procedures were followed, but no illumination was used.

RESULTS AND DISCUSSION

Galvanostatic electrolysis with product analysis

Electrolysis experiments were conducted in 0.5 M $KHCO_3$ with GDEs prepared using unmodified ACF, and iron, nickel, copper, and palladium catalysts supported either on non-activated carbon fibers (CFs) or on ACFs. The ACF support itself exhibited very little activity [*ca* 2.5% current efficiency (CE)] for CO_2 reduction, and hydrogen evolution was the principal reaction. The CF/Fe, CF/Ni and CF/Pd catalysts also showed low activity for CO_2 reduction. These metal catalysts supported on ACF, however, showed significant activity, the highest CE being observed for ACF/Ni, which reduced CO_2 with an overall CE of 45.3%, with CO being produced at 30.2% CE, and formic acid being produced at 15.0% CE. The ACF/Fe catalyst was the next most active, producing formic acid at 9.5% CE. The ACF/Pd catalyst was next, yielding 6.2% CE for CO production. For these metals, it appears that there is a definite enhancement of CO_2 reduction due to the effect of the micropores.

Both CF/Cu and ACF/Cu produced significant amounts of methane, as well as some CO. The CE values for methane and CO production were 6.6% and 3.1% respectively for CF/Cu. In terms of CE for methane production, the activity was actually lower for the ACF/Cu catalyst than for CF/Cu. In terms of current densities (CDs), the values were nearly the same. The partial current densities (PCDs) for CO on ACF/Cu (6.0%) were approximately a factor of six greater than that for CF/Cu, also indicating a definite effect of the micropores for CO_2 reduction on copper catalysts.

Current–potential behavior for hydrogen evolution on GDEs

The PCDs for CO_2 reduction and H_2 evolution for the various metal catalysts supported on ACF were examined as a function of potential (1.6 to −2.0 V vs SCE) in order to understand better the effects of kinetics and mass transport. The PCD values were quite similar for all of the catalysts, with the variations being less than an order of magnitude, when comparing them at the same potential. In addition, the PCD values for hydrogen evolution increased in an exponential fashion for all of the catalysts. This can be seen clearly in the Tafel plots, which are approximately linear (not shown). The slopes for all except ACF/Fe were similar: iron, (440 mV $decade^{-1}$; nickel, 220 mV $decade^{-1}$; copper, 210 mV $decade^{-1}$; palladium, 230 mV $decade^{-1}$.

According to the literature, all of the metals we have examined in the present work (iron, nickel, copper, palladium) exhibit *ca* 120 mV $decade^{-1}$ slopes in alkaline solution for solid electrodes, i.e. the first electron transfer is rate determining.[27] The corresponding exchange CDs differ by as much as two orders of magnitude, however. It appears that all of the slopes (except that for ACF/Fe) obtained in the present work are approximately double those reported for the solid electrodes. The most likely explanation for this phenomenon is diffusion through semi-infinite pores. In that case, the slopes, which are due to mixed control by charge transfer and diffusion, are predicted to be exactly twice the values obtained for solid electrodes.[28] In the present work, the slopes observed for nickel, copper and palladium were indeed approximately twice those reported for solid electrodes, indicating that hydrogen evolution is taking place within the micropores of the ACF. However, it is difficult to explain the fact that the magnitudes of the CDs are all quite similar, even though the exchange CDs reported for the solid electrodes differ significantly.

Current–potential behavior for CO_2 reduction on GDEs

In contrast to the behavior for hydrogen evolution, the PCD values for CO_2 reduction did not vary greatly with potential. However, the values varied considerably for the different catalysts. As already described, the ACF/Ni catalyst exhibited the high-

Copyright © 2001 John Wiley & Sons, Ltd.

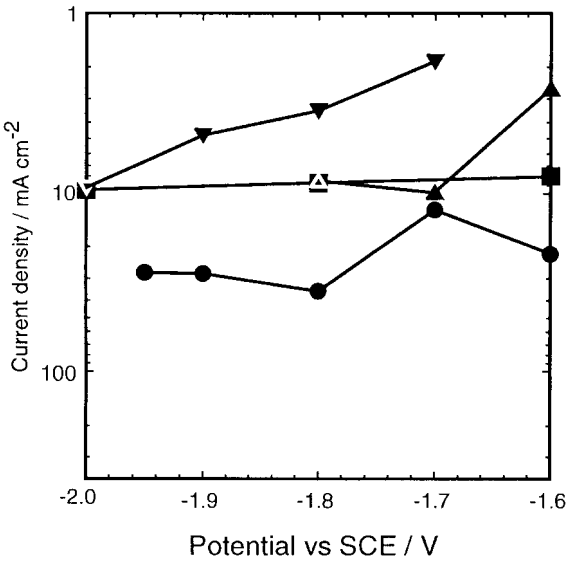

Figure 1 Tafel plots for CO_2 reduction (all products) in CO_2-saturated (1 atm) 0.5 M $KHCO_3$ at ~25 °C for various metallic catalysts supported on ACF in GDEs electrodes: iron (■), copper (▲), nickel (●), and palladium (▼).

est activity. A maximum PCD of *ca* 35 mA cm^{-2} was observed for overall CO_2 reduction at −1.8 V. The activities for the ACF/Fe and ACF/Cu catalysts were lower and similar to each other. The ACF/Pd catalyst showed the lowest activity among these catalysts.

In the Tafel plots for CO_2 reduction, the differences between the catalysts are evident (Fig. 1). ACF/Ni exhibited the largest CD values, which exhibited relatively small variations in this potential range. ACF/Fe exhibited the next highest values, which were also nearly constant, and ACF/Cu also exhibited similar CD values and potential dependence. ACF/Pd exhibited the lowest activity.

Electrode performance optimization for CO_2 reduction on ACF/Ni

We attempted to increase the catalyst loading for ACF/Ni while maintaining a similar electrode structure, in order to maximize the PCD and CE for CO_2 reduction. Specifically, we fabricated an electrode that contained approximately five times as much ACF/Ni as normal (14 mg cm^{-2} instead of 3 mg cm^{-2}). In the potential range from −1.6 to −1.7 V, the PCD values for CO_2 reduction for a lightly loaded electrode were of the same order as those for hydrogen evolution. However, with the heavily loaded electrode, the values for CO_2 reduction exceeded those for hydrogen evolution considerably. For example, at −1.6 V, which was the optimum potential for CO_2 reduction for the more heavily loaded electrode, it exhibited approximately four times as high a PCD for CO_2 reduction (*ca* 65 mA cm^{-2}, which was essentially completely CO production) as for hydrogen evolution (*ca* 15 mA cm^{-2}). This electrode also exhibited approximately three times as high a PCD for CO_2 reduction compared with that for the corresponding more lightly loaded electrode. The CE for hydrogen evolution steadily increased with increasing negative potential, whereas that for CO_2 reduction (CO production) exhibited a maximum of 67% at −1.6 V vs SCE, and decreased with increasing potential.

Based on these results, it is clearly possible to produce mixtures of CO and hydrogen and even to control the ratio. Thus it appears feasible to produce synthesis gas directly. For example, a CO/H_2 ratio of 1:2 is needed for quantitative methanol synthesis, and a 1:1 ratio for Fisher–Tropsch synthesis. By choosing an appropriate potential, the product gas can be optimized for either the methanol system or the Fisher–Tropsch process.

Reaction mechanism for CO_2 reduction

In order to explain the production of CO without significant potential dependence, the most likely approach is to assume that a chemical reaction step is rate determining. For example, based on results from non-aqueous electrolyte, Aylmer-Kelly *et al.* proposed the following mechanism:[29]

$$CO_2(\text{ads}) + e^- \rightarrow CO_2^{\cdot -}(\text{ads}) \quad [1]$$

$$CO_2^{\cdot -} + CO_2 \rightarrow (CO_2)_2^{\cdot -} \quad [2]$$

$$(CO_2)_2^{\cdot -} + e^- \rightarrow (COO^-)_2 \quad [3]$$

Reaction [2] is a candidate for the rate-determining step. It would not normally be expected for such a mechanism to be followed in aqueous solution, but it may be that the environment inside the nanopores is somewhat hydrophobic, due to the enhanced CO_2 adsorption. Amatore and Saveant also examined CO_2 reduction in non-aqueous solution, with and without water present.[30] Three competing pathways were found: (1) oxalate production, as in Eqn [3]; (2) CO production (see below) and (3) formate production via protonation of $CO_2^{\cdot -}$ by water. The

Copyright © 2001 John Wiley & Sons, Ltd.

CO production mechanism involves Eqn [2], the product undergoing either an electrochemical reaction, as in Eqn [3], or chemical reduction via $CO_2^{\cdot -}$. The resulting dianion then decomposes into CO and carbonate.

$$(CO_2)_2^{2-} \rightarrow CO + CO_3^{2-} \quad [4]$$

Vassiliev *et al.* have also proposed a similar mechanism for non-aqueous solution, involving adsorbed species:[31]

$$CO_2^{\cdot -}(ads) + CO_2(ads) \rightarrow (CO_2)_2^{\cdot -}\ (ads) \quad [5]$$

$$(CO_2)_2^{\cdot -}(ads) + e^- \rightarrow (COO^-)_2\ (ads) \quad [6]$$

with Eqn [5] considered to be fast and Eqn [6] to be rate determining. Yet one more possible reaction is:

$$2CO_2^{\cdot -}(ads) \rightarrow CO + CO_3^{2-} \quad [7]$$

To explain the lack of potential dependence, any of Eqns [2], [4], [5], or [7] could be rate determining. It should be noted that the $(CO_2)_2^{\cdot -}$ (ads) species is known to be stable on the Ni(110) surface.[32,33] In the absence of sufficient evidence to choose among these possible rate-determining steps, we propose the simplest one, Eqn [2], which can be written showing more realistic bond angles:[34]

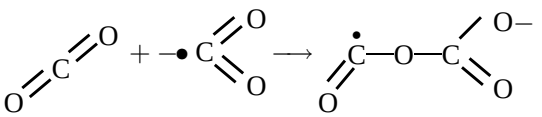
[8]

As we show in a separate publication, the distances between oxygen atoms in CO_2 (232 pm) and $CO_2^{\bullet -}$ (238 pm) match the distance between nickel atoms (248 pm) found along rows on the (110) surface.[26] In addition, these two species can form a T-arrangement, as in Eqn [8], with the bond between the carbon atom of $CO_2^{\cdot -}$ and one of the oxygen atoms of CO_2 being 238 pm, which matches that predicted for the gas-phase adduct (250 pm).[34] Interestingly, a very similar series of mechanistic steps can be proposed to explain our results for the photoelectrochemical reduction of CO_2 in non-aqueous solution (discussed later), but, in that case, a rate-determining electron transfer step is involved.

Copper catalysts supported on both ACFs and CFs have activity for CO_2 reduction. This is not surprising, because copper is known to have activity for methane production even at ambient pressure.[8–10,35] The product distributions for CF/Cu and ACF/Cu are different, however: the main product for CF/Cu is methane, whereas that for ACF/Cu is CO. These results are similar to those of Hori *et al.* on CO_2 reduction on copper electrodes under high CO_2 pressure.[36] Thus it appears that different mechanisms are operative in the two cases.

Electrochemical CO_2 reduction on boron-doped diamond electrodes

As already mentioned in the Introduction, hydrogen evolution is impeded on boron-doped diamond electrode surfaces, which is of potential interest in terms of CO_2 reduction, because of the desire to suppress this reaction. In preliminary work using high-pressure CO_2 in methanol, together with a semiconducting diamond electrode, we found that we were able to reduce CO_2 to various products, with no detectable hydrogen. The major problem that needs to be solved for this approach is that the potentials involved are rather large, on the order of 5 V, due partly to the resistance of the electrode material itself. However, using samples with higher conductivity, hydrogen evolution is no longer negligible, possibly because such samples are of somewhat lower crystalline quality and thus contain defect sites that could catalyze this reaction. This work will be reported in detail in a separate publication.

Current–potential curves for photoelectrochemical CO_2 reduction

Typical current–potential curves for the p-InP photocathode in CO_2 (40 atm)–methanol are shown in Fig. 2. Under illumination, this electrode exhibited large photocurrent densities, exceeding -150 mA cm^{-2}, for potentials more negative than -1.8 V vs Ag QRE (Fig. 2, curve a), whereas the dark current was negligibly small (less than -1 mA cm^{-2}) at potentials down to -2.0 V (curve b). The potential was corrected for the solution resistance, which was measured using an *IR* compensator. The high-pressure CO_2–methanol solution has a high resistance (50 to 70 Ω in our particular cell arrangement). Both the corrected- and uncorrected-potential curves are shown in Fig. 2; the latter is shown as curve c. The initial part of the curve is characterized by an exponentially increasing current. As shown in our previous report, even at higher current densities, the reaction is limited by light intensity and not by mass transport.[25]

Copyright © 2001 John Wiley & Sons, Ltd.

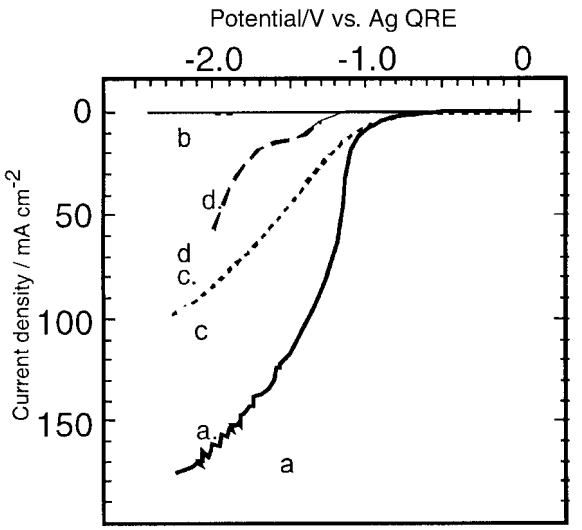

Figure 2 Current–potential curves for CO_2 reduction on p-InP in high-pressure CO_2 (40 atm) in methanol (0.1 M) TBAP at ~25 °C: (a) ohmic drop-corrected curve under illumination; (b) dark current on the same electrode; (c) non-corrected curve; (d) curve obtained for a solid copper electrode in the dark.

The overall reaction is:

$$2CO_2 + 2e^- = CO + CO_3^{2-} \qquad [9]$$

which has an E^0 of −0.555 V vs a normal hydrogen electrode in aqueous solution, based on 1 atm gas pressures and 1 M CO_3^{2-} concentration.[25] Lacking the corresponding value for methanol, we simply use this value. Correcting for the CO_2 pressure (40 atm) yields a value of −0.46 V, and making a further correction to the Ag QRE scale yields a value of −0.78 V. At this potential, we observe a CD of −2 to −3 mA cm^{-2}.

As a comparison, a current–potential curve is also shown for the dark electrochemical reaction on a copper electrode measured under essentially the same conditions (data taken from work of Saeki *et al.*[22]). The current onset is *ca* 0.4 V more negative compared with that for the p-InP photoelectrode (with a larger shift, *ca* 0.7 V for higher CD), showing that, in principle, the bias voltage of a CO_2-producing photoelectrochemical cell based on such an electrode would be significantly smaller than the corresponding non-illuminated electrochemical cell.

For the p-InP electrodes at 40 atm CO_2 pressure, the CE values for CO production were 87–93% in the current range from 50 to 100 mA cm^{-2}, compared with 60% at 1 atm, whereas hydrogen production was suppressed at 40 atm (<5%), compared with that at 1 atm (33%). Thus, a very high selectivity for CO_2 reduction was obtained in CO_2 (40 atm)–methanol at high CD. This result is somewhat similar to those for certain metal electrodes such as silver and gold.[37–39]

Tafel plots for photoelectrochemical CO_2 reduction

The PCD Tafel plots for each of the measured products at 40 atm CO_2 pressure are shown in Fig. 3 for p-InP. It can be seen that the CD values for CO (curve a) and methyl formate (curve b) production exhibited Tafel linearity up to approximately −50 mA cm^{-2}, whereas that for hydrogen evolution (curve c) saturated at lower CD (approximately −3 mA cm^{-2}). At CD greater than −50 mA cm^{-2}, the values for CO and methyl formate production also exhibited saturation, and the total CD saturated as well. The Tafel slope for CO production was approximately −120 mV $decade^{-1}$ at lower CD, as indicated in Fig. 3. This slope is in agreement with those for electrochemical CO_2 reduction to CO reported by several authors for aqueous media[40] and non-aqueous media,[29] as well as that for the photoelectrochemical reaction reported by Bockris

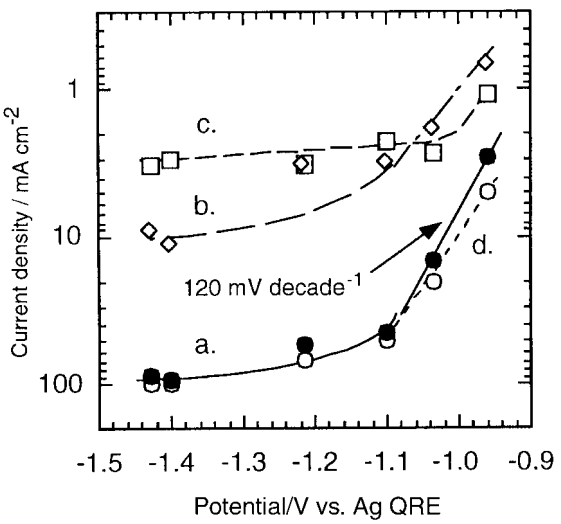

Figure 3 Tafel plots for CO_2 reduction on p-InP in high pressure CO_2 (40 atm) in methanol (0.1 M) TBAP at ~25 °C to various products: (a) CO; (b) methyl formate; (c) hydrogen (d) total current.

Copyright © 2001 John Wiley & Sons, Ltd.

and coworkers using p-CdTe in DMF containing 5% water.[41,42]

Photoelectrochemical reaction mechanism for CO_2 reduction

The following results must be explained: (1) a PCD Tafel slope for CO production of $ca - 120$ mV; (2) the onset of current at a potential (-0.5 V vs Ag QRE) that is much more positive than the E^0 for the CO_2/CO_2^- redox couple [-1.90 V vs the standard hydrogen electrode SHE, or -2.22 V vs Ag QRE], even considering the photoenhancement; (3) the high CE values for CO production, particularly at high CO_2 pressure and negative potentials. The $ca - 120$ mV Tafel slope, (i.e. $-2.3RT/\alpha nF$, where the transfer coefficient $\alpha = 0.5$) is a good indication of a first electron transfer step being rate determining. Slopes close to this value have been obtained for both electrochemical and photoelectrochemical experiments for several different types of electrode that produce mostly CO in non-aqueous solution. Therefore, it appears likely for the first electron transfer to CO_2 (reaction [1]) to be rate determining. However, we argue in our previous publication that reaction [1] cannot be rate determining simply as written, because of point (2), i.e. the early onset of current (a shift in the potential of $ca + 1.7$ V, of which at most 0.7 V could be accounted for by photoenhancement).[25] In order to explain such a shift, we must consider that the $CO_2^{\cdot -}$ radical anion is stabilized on the surface, similar to the case of Ni(110), as discussed above.

There are two key points regarding the gas-phase radical anion dimer species $(CO_2)_2^{\cdot -}$: (1) it is stabilized with respect to dissociation into CO_2 and $CO_2^{\cdot -}$ by 0.58 eV;[34] (2) the electron affinity is positive (+0.9 eV), whereas that for $CO_2^{\cdot -}$ is negative (-0.6 eV).[43] Therefore, with no solvation or adsorption effects, we expect a positive shift of 1.5 V for the E^0 for Eqn [10] compared with the simple reduction of CO_2 to $CO_2^{\cdot -}$:

$$2CO_2 + e^- \rightarrow (CO_2)_2^{\cdot -} \qquad [10]$$

This would put the E^0 in the neighborhood of -0.4 V vs SHE or -0.72 V vs Ag QRE. Of course, any solvation or adsorption effects would modify this. This value appears to be reasonable if we examine the current–potential behavior for p-InP (Fig. 2). Showing this reaction in terms of realistic bond angles:

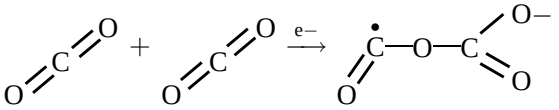

[11]

We have therefore proposed the latter as the rate-determining step in the photoelectrochemical production of CO in CO_2–CH_3OH. The CO_2 and $CO_2^{\cdot -}$ species could reasonably adsorb on the InP (100) surface, because the In—P bond is 254 pm, although there does not exist direct experimental evidence for adsorption. In addition, the indium and phosphorus atoms are arranged in such a way as to allow the appropriate interaction of the CO_2 and $CO_2^{\cdot -}$ species for stabilization.

The high CO yield at high CO_2 pressures and negative potentials can be rationalized, because the stability of the adsorbed $(CO_2)_2^{\cdot -}$ species would be enhanced at high CO_2 pressure. Otherwise, the increasingly strong adsorption of tetrabutylammonium cations with increasing negative potential would tend to inhibit CO_2 adsorption.[44]

CONCLUSIONS

The present work shows that it is possible to enhance the current density, lower the polarization and enhance the selectivity for CO_2 reduction if the appropriate requirements are met, e.g. (1) either high-pressure CO_2 or conditions that mimic high pressure, such as nanopore adsorption; (2) involvement of the CO_2 dimer radical anion, which appears to facilitate greatly the reduction pathways that result in CO production. Interestingly, it appears that similar mechanistic pathways are involved in CO_2 reduction for both the ACF/Ni GDE in aqueous solution and the p-InP photoelectrode in methanol solution.

For the ACF/Ni catalyst, the lack of potential dependence leads us to propose a rate-determining step involving a chemical reaction between CO_2 and the CO_2 radical anion to produce the dimer radical anion. Nickel appears to be a good catalyst because of the known stability of the dimer radical anion on the Ni(110) surface.

For the p-InP (100) photoelectrode, the arrangement of surface atoms is also appropriate for the stabilization of the CO_2 dimer radical anion, and thus the proposed mechanism, involving the

Copyright © 2001 John Wiley & Sons, Ltd.

reduction of two CO_2 molecules to produce this species directly, is reasonable. Most of the experimental results can be explained with this hypothesis, including the high current efficiency for CO production, even out to very negative potentials, under high-pressure CO_2.

Acknowledgements This work was partially supported by a Grant-in-Aid for Scientific Research from the Ministry of Education, Science, Sports and Culture of Japan and was also partially supported by the International Joint Research Program of New Energy and Industrial Technology Development Organization (NEDO).

REFERENCES

1. Halmann MM, Steinberg M. *Greenhouse Gas Carbon Dioxide Mitigation Science and Technology*. Lewis Publishers: Boca Raton, 1999.
2. Furuya N, Matsui K, Motoo S. *Denki Kagaku* 1987; **55**: 787.
3. Furuya N, Matsui K, Motoo S. *Denki Kagaku* 1988; **56**: 980.
4. Furuya N, Yamazaki T, Shibata M. *J. Electroanal. Chem.* 1997; **431**: 39–41.
5. Furuya N, Yamazaki T, Shibata M. *Denki Kagaku* 1998; **66**: 219–220.
6. Furuya N, Matsui K, Motoo S. *Denki Kagaku* 1988; **56**: 288.
7. Furuya N, Matsui K. *J. Electroanal. Chem.* 1989; **271**: 181.
8. Cook RL, Macduff RC, Sammells AF. *J. Electrochem. Soc.* 1990; **137**: 607.
9. Ikeda S, Ito T, Azuma K, Ito K, Noda H. *Denki Kagaku* 1995; **63**: 63.
10. Ikeda S, Ito T, Azuma K, Nishi N, Ito K, Noda H. *Denki Kagaku* 1996; **64**: 69.
11. Hara K, Kudo A, Sakata T, Watanabe M. *J. Electrochem. Soc.* 1995; **142**: L57–L59.
12. Hara K, Sonoyama N, Sakata T. *Bull. Chem. Soc. Jpn.* 1997; **70**: 745–754.
13. Hara K, Sakata T. *Bull. Chem. Soc. Jpn.* 1997; **70**: 571–576.
14. Hara K, Sakata T. *J. Electrochem. Soc.* 1997; **144**: 539–545.
15. Cazorla-Amoros D, Alcaniz-Monge J, Linares-Solano A. *Langmuir* 1996; **12**: 2820–2824.
16. Cazorla-Amoros D, Alcaniz-Monge J, de la Casa-Lillo MA, Linares-Solano A. *Langmuir* 1998; **14**: 4589–4596.
17. Kaneko K, Cracknell R, Nicholson D. *Langmuir* 1994; **10**: 4606–4609.
18. Yamamoto T, Hirota K, Tryk DA, Hashimoto K, Fujishima A, Okawa M. *Chem. Lett.* 1998; **8**: 825–826.
19. Xu J, Granger MC, Chen Q, Strojek JW, Lister TE, Swain GM. *Anal. Chem.* 1997; **69**: 591A–597A.
20. Saeki T, Hashimoto K, Noguchi Y, Omata K, Fujishima A. *J. Electrochem. Soc.* 1994; **141**: L130–L132.
21. Saeki T, Hashimoto K, Kimura N, Omata K, Fujishima A. *Chem. Lett.* 1995; 361–362.
22. Saeki T, Hashimoto K, Fujishima A, Kimura N, Omata K. *J. Phys. Chem.* 1995; **99**: 8440–8446.
23. Saeki T, Hashimoto K, Kimura N, Omata K, Fujishima A. *J. Electroanal. Chem.* 1995; **390**: 77–82.
24. Hirota K, Tryk DA, Hashimoto K, Okawa M, Fujishima A. *J. Electrochem. Soc.* 1998; **145**: L82–L84.
25. Hirota K, Tryk DA, Yamamoto T, Hashimoto K, Okawa M, Fujishima A. *J. Phys. Chem. B* 1998; **102**: 9834–9843.
26. Yamamoto T, Hirota K, Tryk DA, Hashimoto K, Fujishima A, Okawa M. In preparation.
27. Appleby AJ, Kita H, Chemla M, Bronoel G. In *Encyclopedia of Electrochemistry of the Elements*, Bard AJ (Ed.). Marcel Dekker: New York, 1982; vol. **IXA**: 383.
28. DeLevie R. In *Advances in Electrochemistry and Electrochemical Engineering*, Delahay P (Ed.). Interscience Publishers: New York, 1967; vol. **6**: 289.
29. Aylmer-Kelly AWB, Bewick A, Cantrill PR, Tuxford AM. *Faraday Disc. Chem. Soc.* 1973; **56**: 96–107.
30. Amatore C, Saveant J-M. *J. Am. Chem. Soc.* 1981; **103**: 5021–5023.
31. Vassiliev YB, Bagotzky VS, Osetrova NV, Khazova OA, Mayorova N. *J. Electroanal. Chem.* 1985; **189**: 311–324.
32. Freund H-J, Messmer RP. *Surf. Sci.* 1986; **172**: 1–30.
33. Bartos B, Freund H-J, Kuhlenbeck H, Neumann M, Lindner H, Mueller K. *Surf. Sci.* 1987; **179**: 59–89.
34. Rossi AR, Jordan KD. *J. Chem. Phys.* 1979; **70**: 4422–4424.
35. Sammells AF, Cook RL. In *Electrochemical and Electrocatalytic Reactions of Carbon Dioxide*, Sullivan BP, Krist K, Guard HE (Eds.). Elsevier: Amsterdam, 1994; 217–262.
36. Hori Y, Takahashi R, Yoshinami Y, Murata A. *J. Phys. Chem. B* 1997; **101**: 7075–7081.
37. Hori Y, Kikuchi K, Suzuki S. *Chem. Lett.* 1985; 1695–1698.
38. Hori Y, Murata A, Kikuchi K, Suzuki S. *J. Chem. Soc. Chem. Commun.* 1987; 728–729.
39. Hori Y, Wakebe H, Tsukamoto T, Koga O. *Electrochim. Acta* 1994; **39**: 1833–1839.
40. Ohkawa K, Noguchi Y, Nakayama S, Hashimoto K, Fujishima A. *J. Electroanal. Chem.* 1994; **369**: 247.
41. Taniguchi I, Aurian-Blajeni B, Bockris JO'M. *Electrochim. Acta* 1984; **29**: 923–932.
42. Bockris JO'M, Wass JC. *J. Electrochem. Soc.* 1989; **136**: 2521–2528.
43. Bowen KH, Liesegang GW, Sanders RA, Herschbach DR. *J. Phys. Chem.* 1983; **87**: 557–565.
44. Chandrasekaran K, Bockris JO'M. *Surf. Sci.* 1987; **185**: 495–514.

Copyright © 2001 John Wiley & Sons, Ltd.